

TABLE OF CONTENTS

COMMUNICATIONS

Diamond Growth on Thin Ti Wafers Via Chemical Vapor Deposition

Q. Chen, Z. Lin

Nanophase BaFe₁₂O₁₉ Synthesized from a Non-Aqueous Microemulsion with Ba- and Fe-Containing Surfactants

V. Chhabra, M. Lal, A.N. Maitra, P. Ayyub

Second Harmonic Characteristics of Disperse Red 1 Doped Polysulfones

S.K. Lor, H. Hiraoka, P. Yu, L-T. Cheng, G.K.L. Wong

Synthesis of Alumina/Nickel Composite by Electrodeposition of Nickel

Y. Hirata, H. Hatano, H. Kyoda, K. Hamasaki

ARTICLES

YBa₂Cu₃O_{7-δ} on MgO Films Grown by Pulsed Organometallic Beam Epitaxy and a Grain Boundary Junction Application

K.A. Dean, D.B. Buchholz, L.D. Marks, R.P.H. Chang, B.V. Vuchic, K.L. Merkle, D.B. Studebaker, T.J. Marks

Investigation of the Processing Conditions for the Growth of Large Cross Section MPMG YBCO Samples in a Bidimensional Temperature Gradient

F. Frangi, I. Monot, M. Murakami

Poisson's Ratio of Porous and Microcracked Solids: Theory and Application to Oxide Superconductors

M.L. Dunn, H. Ledbetter

Excimer Laser-Induced Doping of Crystalline Silicon Carbide Films

S. Krishnan, G.C. D' Couto, M.I. Chaudhry, S.V. Babu

Changes in Surface Area and Composition During Grinding of Silicon in Environments of Various Quality

K. Tkáčová, N. Stevulová, Z. Bastl, P. Stopka, M. Bálintová

Mechanisms of Intrinsic-Stresses-Generation in Sputtered Amorphous Si:H Films

H. Takahashi, H. Nagata, H. Kataoka, H. Takai

Observation and Analysis of Extended Dislocations in an Al-Pd-Mn Icosahedral Quasicrystal by Transmission Electron Microscopy

J. Feng, R. Wang, M. Dai

Hydrothermally Grown BaZrO₃ Films on Zirconium Metal: Microstructure, X-ray Photoelectron Spectroscopy and Auger Electron Spectroscopy Depth Profiling

V.M. Fuenzalida, M.E. Pilleux

Formation Mechanism and Relaxor Ferroelectric Properties of Lead Lithium Iron Tungstate Ceramics

C-H. Lu, W-S. Hwang

"Square" Hysteresis Loops in Phase Switching Nb-Doped Lead Zirconate Stannate Titanate Thin Films

C.J. Gaskey, K.R. Udayakumar, H.D. Chen, L.E. Cross

The Dielectric Temperature Characteristic of Additives Modified Barium Titanate Having Core Shell Structured Ceramics

Y. Park

The Effect of Stoichiometry on the Microstructure and Properties of Lead Lanthanum Titanate Thin Films

A.R. Khan, S.B. Desu

The Effect of Hydrolysis Catalyst on the Ti Deficiency and Crystallite Size of Sol-Gel-TiO₂ Crystalline Phases

Bokhimi, A. Morales, O. Novaro, T. López, E. Sánchez, R. Gómez

Synthesis and Characterization of LiTaO₃ Thin Films Deposited on Si by the Sol-Gel Method

P.J. Retuert, P.G. Kneuer, O. Wittke, R.E. Avila, G.J. Piderit

Discussion on Microstructure of Chemical Vapor Deposited TiN Films Based on the Calculated Gaseous Concentration Distribution in the Reactor

N. Yoshikawa, A. Kikuchi

Rheology of Aqueous Boehmite-Coated Silicon Nitride Suspensions and Gels

W-H. Shih, L-L. Pwu

Calibration of the Raman Effect in α -Al₂O₃ Ceramic for Residual Stress Measurements

M.R. Gallas, Y.C. Chu, G.J. Piermarini

Effect of Ion Fluence on the Surface Morphology of Single Crystal Magnesium Oxide Implanted with Xenon

W. Jiang, M.G. Norton, D.B. Poker

The Mechanism and Kinetics of the Niobium-Carbon Reaction Under SHS-Like Conditions

C. He, G.C. Stangle

Photooxidative Self-Cleaning Transparent Titanium Dioxide Films on Glass

Y. Paz, Z. Luo, L. Rabenberg, A. Heller

Effect of Composition on Phase Formation and Morphology in Ti - Si_{1-x}Ge_x Solid Phase Reactions

D.B. Aldrich, Y.L. Chen, D.E. Sayers, R.J. Nemanich, S.P. Ashburn, M.C. Öztürk

Effects of Deposition Temperature on the Electrical Properties of Electron Cyclotron Resonance Plasma-Enhanced Chemical Vapor Deposition Ta₂O₅ Film and the Formation of Interfacial SiO₂

I. Kim, J-S. Kim, B-W. Cho, S-D. Ahn, J.S. Chun, W-J. Lee

Extraordinary Adhesion of a Simple Niobium Metal Bonding Structure

H.S. Chen, D.D. Bacon, H.H. Law, G.W. Kammlott, T.C. Wu

Nanoscale Carbon Blacks Produced by CO₂ Laser Pyrolysis

X-X. Bi, J. Jagtoyen, M. Endo, K. Das Chowdhury, R. Ochoa, F.J. Derbyshire, M.S. Dresselhaus, P.C. Eklund

Transmission Electron Microscopy Observation of the Interfacial Reaction Between a Metal Organic Chemical Vapor Deposition BaTiO₃ Thin Film and a (100) MgO Substrate

C.S. Hwang, M.D. Vaudin, G.T. Staaf

On the Elastic Moduli of Nanocrystalline Fe, Cu, Ni and Cu-Ni Alloys Prepared by Mechanical Milling/Alloying

T.D. Shen, C.C. Koch, T.Y. Tsui, G.M. Pharr

An Atomistic Study of Brittle Fracture: Towards Explicit Failure Criteria from Atomistic Modeling

P. Gumbsch

Further Analysis of the Size Effect in Indentation Hardness Tests of Some Metals

M. Atkinson

Interstitial Diffusion Along Twist Grain Boundaries in Cu

M. Nomura, J.B. Adams

Influence of Whisker Volume Fraction on the Creep Behavior of Alumina Composites Reinforced with Silicon Carbide

K. Xia, T.G. Langdon

Equilibrium Phase Diagrams in the System CuO-PbO-Ag

H.K. Liu, S.X. Dou, M. Ionescu, Z.B. Shao, K.R. Liu, L.Q. Liu

In-situ Reduction Kinetics of NiCl₂ in SiO₂ Gel Matrix

A. Basumallick, K. Biswas, G.C. Das, S. Mukherjee

Elastic Properties of Sodium Borovanadate Glasses

S. Muthupari, S. Lakshmi Raghavan, K.J. Rao

Controlling the Particle Size of Amorphous Iron Nanoparticles

X. Cao, Yu. Kolytyn, G. Kataby, R. Prozorov, A. Gedanken

Morphology of α -Hexathieryl Thin-Film-Transistor Films

A.J. Lovinger, D.D. Davis, R. Ruel, L. Torsi, A. Dodabalapur, H.E. Katz

The Topaz to Mullite Transformation on Heating

R.A. Day, E.R. Vance, D.J. Cassidy, J.S. Hartman

ABSTRACTS

COMMUNICATIONS

Diamond Growth on Thin Ti Wafers Via Chemical Vapor Deposition

Q. Chen, Z. Lin

(Chinese Academy of Sciences)

Diamond film was synthesized on thin Ti wafers (as thin as 40 μm) via hot filament chemical vapor deposition (HFCVD). The hydrogen embrittlement of the titanium substrate and the formation of a thick TiC interlayer were suppressed. A very low pressure (133 Pa) was employed to achieve high-density rapid nucleation and thus to suppress the formation of TiC. Oxygen was added to source gases to lower the growth temperature and therefore to slow down the hydrogenation of the thin Ti substrate. The role of the very low pressure during nucleation is discussed, providing insight into the nucleation mechanism of diamond on a titanium substrate. The as-grown diamond films were characterized by scanning electron microscopy (SEM), Raman spectroscopy and x-ray analysis.

Order No.: JA511-001

© 1995 MRS

Nanophase BaFe₁₂O₁₉ Synthesized from a Non-Aqueous Microemulsion with Ba- and Fe-Containing Surfactants

V. Chhabra*, M. Lal*, A.N. Maitra*, P. Ayyub*

(*University of Delhi, *Tata Institute of Fundamental Research)

Ultrafine BaFe₁₂O₁₉ with uniform particle size was synthesized from an alcohol-in-oil (non-aqueous) microemulsion system where the metal ions were supplied by the surfactant (metal di-2-ethylhexylsulfosuccinate) molecules themselves. A mono-disperse, fine-grained precipitate (Ba-Fe oxalate) was ensured by the steric barrier provided by the surfactant monolayer, while the non-aqueous environment promoted stoichiometric co-precipitation. Pure BaFe₁₂O₁₉ was obtained by calcining the oxalate precursor at or above 950°C. Structural and magnetic properties of the resulting ultrafine magnetic material are reported.

Order No.: JA511-002

© 1995 MRS

Second Harmonic Characteristics of Disperse Red 1 Doped Polysulfones

S.K. Lor, H. Hiraoka, P. Yu, L-T. Cheng, G.K.L. Wong

(The Hong Kong University of Science and Technology)

Polysulfones, such as poly(oxy-1,4-phenylenesulfonyl-1,4-phenyleneoxy-1,4-phenyleneisopropylid-ene 1,4-phenylene), poly(phenylene ether sulfone), poly(phenylene sulfone), and aliphatic polysulfone, poly(bicycloheptene sulfone), were employed as a host resin. N-ethyl-N-hydroxyethyl-4-(4' nitrophenylazo)phenylamine (Disperse Red 1) acts as a guest molecule and dispersed in those hosts with a concentration of 5% w/w to 10% w/w. Their second harmonic generation properties were characterized and compared. $\chi_{ijk}^{(2)}$ values obtained varying from 11 pm/V to 21 pm/V. The merits of polysulfones being a host material are its good optical clarity, easy film forming, and fairly high glass transition T_g temperature (140°C to 190°C). Chemically, compared to polyimides they have good resistance to moisture, i.e., they are less vulnerable to hydrolysis. These are good candidates for electro-optical materials.

Order No.: JA511-003

© 1995 MRS

Synthesis of Alumina/Nickel Composite by Electrodeposition of Nickel

Y. Hirata, H. Hatano, H. Kyoda, K. Hamasaki

(Kagoshima University)

Ni²⁺ ions in aqueous solutions were electrochemically deposited within pores of alumina compacts attached to carbon or Pt electrodes at room temperature. The deposition behavior of Ni metal in the pores of alumina compacts was expressed by an empirical power law equation of $W=kt^n$, where W is the weight of Ni deposited, k is the deposition rate constant, t is the deposition time, and n is the experimental constant (0.52–0.56). The shape of Ni deposited was dependent on the geometry of positive electrode.

Order No.: JA511-004

© 1995 MRS

ARTICLES

YBa₂Cu₃O_{7-δ} on MgO Films Grown by Pulsed Organometallic Beam Epitaxy and a Grain Boundary Junction Application

K.A. Dean*, D.B. Buchholz*, L.D. Marks*, R.P.H. Chang*, B.V. Vuchic*, K.L. Merkle*, D.B. Studebaker*, T.J. Marks*
 (*Northwestern University, *Argonne National Laboratory)

MgO films and YBa₂Cu₃O_{7-δ}/MgO multilayer films were developed with the pulsed organometallic beam epitaxy (POMBE) growth technique, and grain boundary junctions were fabricated from the films to demonstrate the utility of the multilayers. High-quality MgO films were grown on LaAlO₃ substrates by POMBE using a Mg(dpm)₂ precursor. MgO crystallinity, as assessed by x-ray diffraction rocking curves, improved with the use of CuO_x or YBa₂Cu₃O_{7-δ} buffer layers. YBa₂Cu₃O_{7-δ} films grown on the MgO layer by POMBE exhibited a T_{c0} of 83 K and a J_c(12 K) exceeding 10⁶ A/cm² for applied magnetic fields up to 3x10⁴ gauss. Grain boundary junctions were formed by growing YBa₂Cu₃O_{7-δ} on MgO films that had been pretreated with a simple sputtering technique. This sputtering induces a controlled, 45° grain boundary in subsequently deposited YBa₂Cu₃O_{7-δ} films. The resulting boundary showed weak-link current-voltage behavior and an I_cR_n product of 52 μV at 10 K, demonstrating that sputter-induced grain boundary junctions are compatible with multilayer technology.

Order No.: JA511-005

© 1995 MRS

Investigation of the Processing Conditions for the Growth of Large Cross Section MPMG YBCO Samples in a Bidimensional Temperature Gradient

F. Frangi, I. Monot, M. Murakami

(Superconductivity Research Laboratory-ISTEC)

A bidirectional gradient furnace with sample displacement was used for the growth of large MPMG YBCO samples. The optimization of the macrogranular structure with consequent extension of the central part of the sample, characterized by large aligned domains, was studied. Considering the large cross section of our samples, we studied the combined effects of different ratios between the longitudinal and transversal temperature gradients, different pulling rates (R = 0, 0.5, 1 and 2 mm/h) and one or more stages at the beginning of the sample growth on grain nucleation, dimension and orientation. Different mechanical pretreatments of sample surfaces were also tested in order to control domain nucleation. We obtained 20x25x45 mm³ samples with low misoriented extended domains. Moreover we were able to vary their c axis directions from perpendicular to parallel with respect to the sample length.

Order No.: JA511-006

© 1995 MRS

Poisson's Ratio of Porous and Microcracked Solids: Theory and Application to Oxide Superconductors

M.L. Dunn*, H. Ledbetter†

(*University of Colorado, †National Institute of Standards and Technology)

We present a theoretical study of the effective Poisson's ratio of elastic solids weakened by porosity and microcracks. Explicit expressions of the effective Poisson's ratio are obtained through the Mori-Tanaka mean-field approach as applied to macroscopically isotropic solids containing randomly distributed and randomly oriented spheroidal pores. We focus on the influence of pore shape and concentration and devote special attention to the limiting cases of spherical, penny-shape, and needle-shape pores. A key result of this study is that the effective Poisson's ratio depends only on the pore concentration and pore shape, and Poisson's ratio of the bulk solid. In other words, it is independent of any other elastic constants of the bulk solid. Also, the ratio of the shear and bulk moduli behaves similarly. Unlike other elastic constants, which monotonically decrease with pore concentration, Poisson's ratio may increase, decrease, or remain unchanged as a function of pore concentration, depending on the pore shape and Poisson's ratio of the bulk solid. We discuss ramifications of these findings with regard to the elastic constants of oxide superconductors, especially the bismuth cuprates, which show unusually low Poisson's ratios. We also discuss these low Poisson's ratios, including the possibility of negative Poisson's ratios.

Order No.: JA511-007

© 1995 MRS

Excimer Laser-Induced Doping of Crystalline Silicon Carbide Films

S. Krishnan, G.C. D' Couto, M.I. Chaudhry, S.V. Babu

(Clarkson University)

0.25 μm thick, single crystal, n-type, silicon carbide (β-SiC) films thermally grown on p-type Si(100) were doped with boron by using KrF excimer laser radiation and a spin-on dopant with a boron concentration of 10²⁰/cm³. The threshold fluence for the doping to occur was approximately 0.08 J/cm². Similarly, p-SiC/n-SiC diodes were fabricated by laser-induced doping of single crystal β-SiC (n-type, 6 μm thick) films on n-type Si(100). The diodes obtained at 0.25 J/cm² showed good rectifying characteristics. The threshold fluence for surface modification and/or ablation was approximately 0.3 J/cm², indicating that doping and diode formation have to be accomplished within the fluence window of 0.08 J/cm²–0.3 J/cm² for these films.

Order No.: JA511-008

© 1995 MRS

Changes in Surface Area and Composition During Grinding of Silicon in Environments of Various Quality

K. Tkáčová*, N. Števelová*, Z. Bastl†, P. Stopka#, M. Bálintová*
 (*Slovak Academy of Sciences, †J. Heyrovský Institute of Physical Chemistry, #Academy of Sciences of the Czech Republic)

Changes in particle size, surface properties and composition brought about by planetary grinding of silicon in air and various permissibility liquids were investigated. Using a variety of spectroscopic techniques (ESR, IRS, XPS) a mechanically induced surface oxidation was proved. While grinding in air and organic liquids a part of the centers originating from dangling orbitals on Si^{III} are preserved, the properties of water ground silicon are fully governed by the oxide surface shell. The most effective particle size reduction and surface protection can be reached by grinding in non-polar liquids.

Order No.: JA511-009

© 1995 MRS

Mechanisms of Intrinsic-Stresses-Generation in Sputtered Amorphous Si:H Films

H. Takahashi*, H. Nagata*, H. Kataoka*, H. Takai†

(*Sumitomo Osaka Cement Co., Ltd., †Tokyo Denki University)

The relation between stresses of sputtered a-Si:H films and the film deposition conditions are investigated. The film stresses change from a large compressive stress of 1000 MPa to an almost stress-free one; they arise from distortions of the Si network via the following two mechanisms. The first result from the inclusion of the Ar sputtering gas into the films which provide volume-expansion of the film network. The second is due to structural disorders, such as a deviation of the Si bond angle which is generated during the deposition processes. Moreover, it is found that Si-H terminations in the films contribute to reducing the film stresses because the Si-H termination breaks and relaxes the Si network. These effects can be realized as long as the Si-H terminations are homogeneously distributed in the films.

Order No.: JA511-010

© 1995 MRS

Observation and Analysis of Extended Dislocations in an Al-Pd-Mn Icosahedral Quasicrystal by Transmission Electron Microscopy

J. Feng, R. Wang, M. Dai

(Wuhan University and Chinese Academy of Sciences)

Extended dislocations including partial dislocations and a stacking fault in Al₇₀Pd₂₀Mn₁₀ icosahedral quasicrystal have been observed and identified for the first time. The diffraction contrast and defocus convergent beam electron diffraction experiments show that the dissociation of the extended dislocations is of the form 1/2<1 -2.0 0 -2 1>6 1/4 <1 -3 1 -1 -1 1>+ 1/4<1 -1 -1 1 -3 1> with a stacking fault between these two partial dislocations. For the partial dislocations, the Burgers vector components in physical space b_{part}^{||} are along different five-fold axes with a magnitude of 0.17 nm, which is about one seventh of that in complementary space. For the perfect dislocation, the Burgers vector component in physical subspace b_{perf}^{||} is along a two-fold axis with a magnitude of 0.183 nm, which is about an eleventh of that in complementary space.

Order No.: JA511-011

© 1995 MRS

Hydrothermally Grown BaZrO₃ Films on Zirconium Metal: Microstructure, X-ray Photoelectron Spectroscopy and Auger Electron Spectroscopy Depth Profiling

V.M. Fuenzalida, M.E. Pilleux
(Universidad de Chile FCFM)

BaZrO₃ films were grown on zirconium metal substrates by immersing thin Zr foils in an alkaline solution under hydrothermal conditions. The films were produced at temperatures ranging from 200°C to 270°C in a 0.25M barium hydroxide solution for 3 to 8 hours. The resulting films did not have visible pores or defects, and displayed a grain structure which depended on the treatment conditions, especially temperature. X-ray photoelectron and Auger spectroscopies revealed that: (a) after removing the surface layer, films were clean, not displaying OH groups nor carbon contamination; (b) the Ba concentration steadily decreased as the depth increased, and did not behave as in BaTiO₃ or SrTiO₃ films prepared under similar conditions; and (c) the BaZrO₃/Zr interface was very broad. Grazing angle x-ray diffraction analysis showed BaZrO₃(cubic), ZrO₂(hexagonal), and Zr(hexagonal), suggesting a layered structure: BaZrO₃/ZrO₂/Zr. The relative dielectric constant was ≈70 and was independent on the frequency between 100Hz and 1MHz. The dielectric loss factor (tanδ) was between 0.01 and 0.02. Dielectric breakdown occurred between 25 and 40MVm⁻¹.

Order No.: JA511-012 © 1995 MRS

Formation Mechanism and Relaxor Ferroelectric Properties of Lead Lithium Iron Tungstate Ceramics

C-H. Lu, W-S. Hwang
(National Taiwan University)

The formation mechanism and ferroelectric properties of Pb(Li_{1/4}Fe_{1/4}W_{1/2})O₃ prepared by solid-state reaction have been investigated in this study. The formation processes of Pb(Li_{1/4}Fe_{1/4}W_{1/2})O₃ are characterized to be an initial reaction of lead tungstates PbWO₄ and Pb₂WO₅ at a low temperature range, followed by a subsequent reaction to produce Pb(Li_{1/4}Fe_{1/4}W_{1/2})O₃ from above 650°C. Through a two-stage calcination (700°C/quenching regrinding-710°C/8h), a nearly single phase of Pb(Li_{1/4}Fe_{1/4}W_{1/2})O₃ is obtained. This compound exhibits a cubic perovskite structure (a = 8.0113 Å) with a partially ordering arrangement of B-site cations. Above 720°C, Pb(Li_{1/4}Fe_{1/4}W_{1/2})O₃ becomes thermodynamically unstable and gradually decomposes in forming elongated Pb₂WO₅ grains, thereby resulting in non-homogeneous microstructure. As the AC frequency increases, the maximum dielectric permittivity of Pb(Li_{1/4}Fe_{1/4}W_{1/2})O₃ significantly decreases; in addition, the corresponding temperature increases. The strong frequency dependence of dielectric properties, as well as the critical exponent and diffuseness evaluated through a modified permittivity-temperature equation proposed in this study, verify the relaxor characteristics of Pb(Li_{1/4}Fe_{1/4}W_{1/2})O₃.

Order No.: JA511-013 © 1995 MRS

"Square" Hysteresis Loops in Phase Switching Nb-Doped Lead Zirconate Stannate Titanate Thin Films

C.J. Gaskey, K.R. Udayakumar, H.D. Chen, L.E. Cross
(The Pennsylvania State University)

Niobium doped lead zirconate stannate titanate thin films have been prepared by a modified sol-gel spin on technique, utilizing the hydrolysis-resistant precursor lead acetylacetonate. Films of compositions in the antiferroelectric tetragonal and antiferroelectric orthorhombic phases were prepared and phase switched with the application of appropriate electric fields. A distinctly "square" hysteresis response was observed in a low titanium, low tin, orthorhombic composition, with a maximum polarization, P_{max}, of 40 μC/cm² and switching field values of E_f = 175 kV/cm and E_a = 75 kV/cm, while varying degrees of squareness, along with lower polarizations and switching fields, were observed in the higher tin, tetragonal compositions. Electric field-induced strains of up to 0.33% have been measured in the orthorhombic composition, with tunable electromechanical coefficients. Film properties showed only slight variation with electrode size over a range of diameters from 0.8 mm to 6.35 mm; large area electrodes are vital for practical actuator and

sensor devices. With a capacitance density of 30–35 μF/cm², films of the orthorhombic composition are promising as power plane decoupling capacitors in multi-chip modules.

Order No.: JA511-014

© 1995 MRS

The Dielectric Temperature Characteristic of Additives Modified Barium Titanate Having Core Shell Structured Ceramics

Y. Park
(Korea Advanced Institute of Science and Technology)

The dielectric temperature characteristics and microstructures of BaTiO₃ based ceramics sintered with additives such as Sm₂O₃, CeO₂ and Bi₂O₃:Nb₂O₅ were investigated using TEM, XRD and EDS. For Sm₂O₃ modified BaTiO₃ ceramic whose additives were uniformly distributed in grains, the ferroelectric transition temperature (T_c) was shifted to a lower temperature, while the transition temperatures (T₁ and T₂) were shifted to a higher temperature. The additions of CeO₂ and Bi₂O₃:PbO to BaTiO₃ formed the chemical inhomogeneity which was composed of grain-core, grain-shell and concentration gradient region. The dielectric curve vs. temperature of CeO₂ modified BaTiO₃ has the shape of one strong peak, whereas BaTiO₃ ceramics sintered with Bi₂O₃:Nb₂O₅ exhibit the broad dielectric constant at the low temperature region and 130°C ferroelectric transition peak. The dielectric temperature characteristics of additives modified BaTiO₃ were determined in terms of the chemical inhomogeneity and stress induced by the difference of the unit cell volume between grain-core and grain-shell.

Order No.: JA511-015

© 1995 MRS

The Effect of Stoichiometry on the Microstructure and Properties of Lead Lanthanum Titanate Thin Films

A.R. Khan, S.B. Desu
(Virginia Polytechnic Institute and State University)

Thin films of lead lanthanum titanate (PLT) corresponding to 28 at.% of La were prepared by metalorganic decomposition (MOD) process. The films were fabricated from two solutions of different composition. The composition of the first solution was determined assuming that the incorporation of La³⁺ in the PbTiO₃ structure gives rise to A-site or Pb vacancies whereas for the composition of the other solution the creation of B-site or Ti vacancies was assumed. The effect of excess lead on the microstructure and the optical and electrical properties was studied for 0% to 20% of excess PbO. The x-ray diffraction patterns of all films at room temperature indicated a cubic structure with lattice constant of 3.92 Å. Optical and electrical measurements showed that the films made assuming B-site vacancies had better properties. In general, excess PbO was found to improve the optical transmittance as well as the electrical properties of films. However, in films assuming the formation of B-site vacancies, the improvement in electrical properties occurred only up to 5–10% of excess PbO, while higher PbO additions had a deleterious effect. The films had high resistivity, good relative permittivity, low loss, very low leakage current density, and high charge storage density. A type-B film with 10% excess Pb had a relative permittivity of 1340 at 100 kHz and a charge storage density of around 16.1 μC/cm² at a field of 200 kV/cm at room temperature.

Order No.: JA511-016

© 1995 MRS

The Effect of Hydrolysis Catalyst on the Ti Deficiency and Crystallite Size of Sol-Gel-TiO₂ Crystalline Phases

Bokhimi*, A. Morales*, O. Novaro*, T. López*, E. Sánchez*, R. Gómez*
(*National University of Mexico-UNAM, *Universidad Autónoma Metropolitana-Iztapalapa and Universidad de Guanajuato)

We prepared sol-gel titania by using different hydrolysis catalysts, and characterized it by x-ray powder diffraction. The structure of the crystalline phases—brookite, anatase and rutile—in the samples annealed between 70 and 900°C was refined by using the Rietveld technique. From the refinement we obtained the structure parameters, the concentration of each phase and their average crystallite size. These quantities and their evolution with temperature depended on the hydrolysis catalyst. Anatase and rutile were deficient in Ti, suggesting that their crystalline structure contained hydrogen forming OH⁻ ions inside.

In anatase this deficiency depended on its crystallite size, but it was constant in rutile. When anatase was annealed, it dehydroxylated producing either crystallite growing up or its conversion into rutile. From the analysis we also found the conditions for obtaining single phase samples that could be used as precursors for making up titania single-phase thin films.

Order No.: JA511-017

© 1995 MRS

Synthesis and Characterization of LiTaO₃ Thin Films Deposited on Si by the Sol-Gel Method

P.J. Retuert*, P.G. Kneuer*, O. Wittke*, R.E. Avila*, G.J. Piderit*
(*Universidad de Chile, *Comisión de Energía Nuclear)

Polycrystalline LiTaO₃ (LT) thin films have been prepared on (001)Si substrates by the sol-gel method. A Li-Ta double alkoxide prepared from lithium and tantalum alkoxide precursors was spin coated on Si and heated up to 950°C. The dependence of the film quality upon the process variables: alkoxide concentration before hydrolysis, the water to alkoxide ratio, and the final double alkoxide concentration has been established. Preferential alignment of the (104) LT planes was observed parallel to the (100)Si surface. Most films present resistivities of the order of 30 KΩ·cm and breakdown field in excess of 200 KV/cm.

Order No.: JA511-018

© 1995 MRS

Discussion on Microstructure of Chemical Vapor Deposited TiN Films Based on the Calculated Gaseous Concentration Distribution in the Reactor

N. Yoshikawa, A. Kikuchi
(Tohoku University)

TiN films were chemical vapor deposited on the inner wall of a tubular reactor. Films deposited in the upstream region of the reactor consisted of small and sharp crystals with (111)-preferred orientation or random orientation. On the other hand, films deposited in the downstream region or at lower partial pressure of TiCl₄ consisted of columnar crystals with (110)-preferred orientation, having polyhedral shapes on the surface.

For the films deposited under different conditions at different axial positions, relationships were investigated between the temperature, the calculated concentrations on the substrate and the degree of preferred orientation of the films. As a result, it was shown that formation of films with (110)-preferred orientation is related with the conditions of high temperature and low partial pressure of TiCl₄.

Films deposited at the higher gas flow rate had the lower degrees of (110)-preferred orientation. Decrease in partial pressure of TiCl₄ along the axial direction in the reactor was calculated to be smaller at higher gas flow rate, and provided the suitable conditions for deposition of the films having small and sharp crystals.

Order No.: JA511-019

© 1995 MRS

Rheology of Aqueous Boehmite-Coated Silicon Nitride Suspensions and Gels

W-H. Shih, L-L. Pwu
(Drexel University)

The rheological properties of boehmite-coated silicon nitride aqueous suspensions and gels are reported. In unidirectional rheological tests, it was found that the boehmite coating reduces the viscosity of the suspensions over a wide range of shear rates and volume fractions of particles. The suspension shear stress as a function of shear rate can be described by the Bingham model and the Bingham yield stresses of boehmite-coated silicon nitride suspensions are lower than those of the uncoated suspensions. The reduction in the viscosity and the Bingham yield stress is attributed to a shallower secondary minimum in the DLVO potential between coated particles than that for uncoated silicon nitride particles. Moreover, at low values of pH, the coated silicon nitride suspensions gelled over time, and the viscoelastic behavior of the gels were studied by dynamic oscillatory tests. It was found that the shear modulus (G') and loss modulus (G'') remain constant up to a certain strain amplitude, γ_c , beyond which G' and G'' begin to vary. The value of G' in the linear region increases exponentially whereas γ_c decreases

exponentially with volume fraction of particles of coated silicon nitride particles. The exponential behavior of the shear modulus G' of the gels is similar to the exponential pressure-density relationship found in the previous pressure filtration study, indicating that particulate rearrangement occurs as volume fraction of particles is increased.

Order No.: JA511-020

© 1995 MRS

Calibration of the Raman Effect in α -Al₂O₃ Ceramic for Residual Stress Measurements

M.R. Gallas, Y.C. Chu, G.J. Piermarini
(National Institute of Standards and Technology)

The pressure shifts of the 418 and 379 cm⁻¹ Raman lines of polycrystalline α -Al₂O₃ ceramic were measured at room temperature to 3190 MPa. A diamond anvil high pressure cell was used in conjunction with a microRaman spectrometer system. Pressures were measured by the ruby fluorescence method. Distilled water was used as the pressure transmitting medium. The pressure dependence of the wavenumber for the hydrostatic range (to 1585 MPa) was found to be 0.00220 ± 0.00007 cm⁻¹ MPa⁻¹ for the 418 cm⁻¹ Raman line and 0.0011 ± 0.0001 cm⁻¹ MPa⁻¹ for the 379 cm⁻¹ line. Both shifts are based on a linear least squares fit to the data within a 95% confidence interval. Measurements which included the nonhydrostatic regime (to 3190 MPa) gave similar shifts, but with almost twice the uncertainty. Absolute residual stresses in alumina ceramics are in the 200 to 600 MPa range with higher values, 1790 MPa, reported for single crystal alumina. For the 418 cm⁻¹ Raman line, these values correspond to shifts of 0.4, 1.4 and 3.9 cm⁻¹, respectively. The sensitivity of the microRaman technique is sufficient to detect and measure residual stresses of this magnitude.

Order No.: JA511-021

© 1995 MRS

Effect of Ion Fluence on the Surface Morphology of Single Crystal Magnesium Oxide Implanted with Xenon

W. Jiang*, M.G. Norton*, D.B. Poker*
(*Washington State University, *Oak Ridge National Laboratory)

The surface morphology of (001)-oriented single crystal magnesium oxide (MgO) implanted with xenon ions has been examined using atomic force microscopy. It was found that at the lowest fluence used in this study (1.0×10^{14} /cm²), slight roughening of the (001) surface occurred. The magnitude of this roughening remained fairly constant with increases in fluence in the range 1.0×10^{14} /cm² to 3.0×10^{16} /cm². Implantation at fluences of $\geq 1.0 \times 10^{17}$ /cm² caused significant surface roughening with the concomitant formation of micron-sized blisters. The appearance of some of these blisters resembles the rosette pattern which is also observed when the cleaved surfaces of MgO crystals are etched following indentation using a spherical indenter. This observation suggests that these blisters are formed by the growth of xenon inclusions, during implantation, by a dislocation loop punching mechanism.

Order No.: JA511-022

© 1995 MRS

The Mechanism and Kinetics of the Niobium-Carbon Reaction Under SHS-Like Conditions

C. He, G.C. Stangle
(New York State College of Ceramics at Alfred University)

The mechanism and kinetics of the chemical reaction between Nb(s) and C(s) under SHS-like (or combustion synthesis-like) conditions has been studied. Experiments were designed and conducted in order to produce a transport-resistance-free reaction between Nb and C under time-temperature conditions that are characteristic of the combustion synthesis process. To do so, a reaction couple, consisting of carbon and either a thin niobium foil or a fine niobium wire, was used. The effects of the temperature history and the formation of a liquid phase on the reaction were studied. In addition, theoretical experiments of the reaction were also conducted. The results showed that at high temperatures, layered niobium carbide phases formed in a direction that was parallel to the original carbon niobium interface. As might be expected, local melting played a very significant role in the reactions. The mechanism and kinetics of these reactions provide a fundamental understanding of the manner and rate by which a powder based Nb/C

SHS process takes place, and, by extension, to a large, general class of solid-solid material synthesis processes that are based on the SHS (or combustion synthesis) process.

Order No.: JA511-023

© 1995 MRS

Photooxidative Self-Cleaning Transparent Titanium Dioxide Films on Glass

Y. Paz, Z. Luo, L. Rabenberg, A. Heller
(The University of Texas at Austin)

In the context of studying the feasibility of photocatalytically self-cleaning windows and windshields, clear, abrasion-resistant photocatalytic films of TiO₂ were formed on soda lime glass and on fused quartz by a sol-gel process. The rate of photooxidation of contaminant deposits was estimated by measuring the rate of decrease in the integrated IR absorbance associated with the C-H stretching vibrations of a thin solution-cast film of stearic acid under 365 nm (2.4 mW/cm²) or 254 nm (0.8 mW/cm²) irradiation. Approximately 3x10⁻⁴ stearic acid molecules were stripped per 365 nm photon in either front or back-illuminated soda lime glass, and 6x10⁻⁴ molecules when the films were coated on fused quartz. For thin TiO₂ films on fused quartz, the rate of photooxidation, normalized by the number of photons absorbed per unit area, was independent of the wavelength. In contrast, for films on soda lime glass, the rate of photooxidation, when similarly normalized, was higher for the less penetrating wavelength. The reduced photoactivity on glass at the deeply penetrating wavelength (365 nm), as well as the greater photoefficiency on quartz than on glass, are attributed to diffusion of sodium oxide from the glass into the inner glass contacting zone of the TiO₂ layer.

Order No.: JA511-024

© 1995 MRS

Effect of Composition on Phase Formation and Morphology in Ti - Si_{1-x}Ge_x Solid Phase Reactions

D.B. Aldrich, Y.L. Chen, D.E. Sayers, R.J. Nemanich, S.P. Ashburn, M.C. Öztürk
(North Carolina State University)

The effects of Si_{1-x}Ge_x alloy composition on the Ti - Si_{1-x}Ge_x solid phase reaction have been examined. Specifically, effects on the titanium germanosilicide phase formation sequence, C54 Ti(Si_{1-y}Ge_y)₂ nucleation temperature, and C54 Ti(Si_{1-y}Ge_y)₂ morphology were examined. It was determined that the Ti - Si_{1-x}Ge_x reaction follows a "Ti-Si like" reaction path for Si-rich Si_{1-x}Ge_x alloys, and follows a "Ti-Ge like" reaction path for Ge rich Si_{1-x}Ge_x alloys. The coexistence of multiple titanium germanosilicide phases were observed during Ti - Si_{1-x}Ge_x reactions for Si_{1-x}Ge_x alloys in an intermediate composition range. The morphology and stability of the resulting C54 germanosilicides were directly correlated to the Ti - Si_{1-x}Ge_x reaction path. Smooth continuous C54 titanium germanosilicide was formed for samples with Si_{1-x}Ge_x compositions in the "Ti-Si like" regime. Discontinuous islanded C54 germanosilicides were formed for samples with Si_{1-x}Ge_x compositions in the mixed phase and "Ti-Ge like" regimes. Using rapid thermal annealing techniques it was found that the C54 titanium germanosilicides were stable to higher temperatures. This indicated that the morphological degradation occurs after C54 phase formation. The C54 Ti(Si_{1-x}Ge_x)₂ formation temperature was examined as a function of alloy composition and was found to decrease by ≈70°C as the composition approached x=0.5. An optimum Si_{1-x}Ge_x alloy composition range of 0≤x≤0.36 was determined for the formation of stable-, continuous-, low-resistivity-C54 titanium germanosilicide films from the solid phase reaction of Ti and Si_{1-x}Ge_x alloy. The results were described in terms of the relevant nucleation processes.

Order No.: JA511-025

© 1995 MRS

Effects of Deposition Temperature on the Electrical Properties of Electron Cyclotron Resonance Plasma-Enhanced Chemical Vapor Deposition Ta₂O₅ Film and the Formation of Interfacial SiO₂

I. Kim, J-S. Kim, B-W. Cho, S-D. Ahn, J.S. Chun, W-J. Lee
(Korea Advanced Institute of Science and Technology)

High-quality Ta₂O₅ thin films for high-density memory devices were prepared at low temperatures by electron cyclotron resonance plasma-enhanced CVD (ECR-PECVD) without post-annealing treatment. The effects of deposition temperature on the microstructure, composition

and electrical properties of the dielectric films were studied. The increase in deposition temperature from 145°C to 205°C improved the stoichiometry of the Ta₂O₅ thin films. As a consequence, E_{BD} increased from 3.3 MV/cm to 4.4 MV/cm, and ε_{Ta2O5} increased from 14 to 25. Interfacial SiO₂ layer was observed by cross-sectional TEM and its effects on the electrical properties of the overall dielectric film were also studied. The incubation period in which interfacial SiO₂ grows was discussed with regard to reactivity between oxygen and Si substrate.

Order No.: JA511-026

© 1995 MRS

Extraordinary Adhesion of a Simple Niobium Metal Bonding Structure

H.S. Chen, D.D. Bacon, H.H. Law, G.W. Kammlott, T.C. Wu

(AT&T Bell Laboratories)

Extraordinary adhesion of a Nb-base/Au-Sn metallization structure on a SiO₂/Si substrate has been observed by a tensile pull test. The metallization bond fails mostly via fracture through either the Si substrate or epoxy adhesive. The intrinsic adhesion pull strength of the metallization scheme is concluded to be greater than 10 kpsi, and the adhesion exceeds the Si-Si cohesive strength. The Nb-Si and Nb-O bonds at the interface are thermodynamically stable.

Order No.: JA511-027

© 1995 MRS

Nanoscale Carbon Blacks Produced by CO₂ Laser Pyrolysis

X-X. Bi*, J. Jagtoyen*, M. Endo*, K. Das Chowdhury#, R. Ochoa*, F.J. Derbyshire*, M.S. Dresselhaus#, P.C. Eklund*

(*University of Kentucky, *Shinshu University,

#Massachusetts Institute of Technology)

CO₂ laser pyrolysis has been used to synthesize carbon black (particle dia. ~30 nm) via a catalytically driven pyrolysis of benzene vapor. The H:C ratio is found to be ~1:10, which is unusually high for carbon blacks. Subsequent heat treatment of the "laser black" to temperatures up to ~2800°C produces well-graphitized faceted particles with central polygonal cavities. High resolution TEM lattice imaging, Raman scattering and x-ray diffraction have been used to characterize the morphological structure of these carbon particles in their as-synthesized and heat-treated forms. Furthermore, KOH treatment at ~800°C has been employed to activate the as-synthesized particles, producing a tenfold increase in the surface area from 50 to 700 m²/g. Possible pore structures generated during this activation process have been identified by high resolution TEM imaging.

Order No.: JA511-028

© 1995 MRS

Transmission Electron Microscopy Observation of the Interfacial Reaction Between a Metal Organic Chemical Vapor Deposition BaTiO₃ Thin Film and a (100) MgO Substrate

C.S. Hwang*, M.D. Vaudin*, G.T. Stauff*

(*National Institute of Standards and Technology,

*Advanced Technology Materials, Inc.)

Cross-sectional and plan-view transmission electron microscopy were used to characterize a BaTiO₃ thin film deposited on a (100) MgO single-crystal substrate at 1000°C. The major observations were: interdiffusion between the film and substrate; a large number of antiphase boundaries in the BaTiO₃; a two-phase microstructure in the thin film composed of perovskite BaTiO₃ and a second non-perovskite phase, Ba₂MgTi₅O₁₃ (2:1:5); and a well defined orientation relationship between the 2:1:5 and BaTiO₃ phases. We propose a mechanism for the formation of the 2:1:5 phase based on the similarities between the crystal structure of this phase and the structure of (210) antiphase boundaries in BaTiO₃.

Order No.: JA511-029

© 1995 MRS

On the Elastic Moduli of Nanocrystalline Fe, Cu, Ni and Cu-Ni Alloys Prepared by Mechanical Milling/Alloying

T.D. Shen*, C.C. Koch*, T.Y. Tsui*, G.M. Pharr*

(*North Carolina State University, *Rice University)

The Young's moduli of nanocrystalline Fe, Cu, Ni and Cu-Ni alloys prepared by mechanical milling/alloying have been measured by the nanoindentation technique. The results indicate that the Young's moduli of nanocrystalline Cu, Ni and Cu-Ni alloys with a grain size ranging from 17 to 26 nm are similar to those of the corresponding polycrystals. The

dependence of Young's modulus of nanocrystalline Fe on grain size corresponds well to a theoretical prediction which suggests that the change in Young's and shear moduli of nanocrystalline materials, free of porosity, with a grain size larger than about 4 nm should be very limited (<10%). It is likely that reported large decreases in Young's and shear moduli of nanocrystalline materials prepared by gas condensation/vacuum consolidation result from a relatively large volume fraction of pores.

Order No.: JA511-030

© 1995 MRS

An Atomistic Study of Brittle Fracture: Towards Explicit Failure Criteria from Atomistic Modeling

P. Gumbsch

(Max-Planck-Institut für Metallforschung)

Atomistic techniques are used to study brittle fracture under opening mode and mixed mode loading conditions. The influence of the discreteness of the lattice and of the lattice trapping effect on crack propagation is studied using an embedded atom potential for nickel to describe the crack tip. The recently developed FEAt (Finite Element-Atomistic) coupling scheme provides the atomistic core region with realistic boundary conditions. Several crystallographically distinct crack tip configurations are studied and commonly reveal that brittle cracks under general mixed mode loading situations follow an energy criterion (G-criterion) rather than an opening-stress criterion (KI-criterion). However, if there are two competing failure modes, they seem to unload each other, which leads to an increase in lattice trapping. Blunted crack tips are studied in the last part of the paper and are compared to the atomically sharp cracks. Depending on the shape of the blunted crack tip, the observed failure modes differ significantly and can drastically disagree with what one would anticipate from a continuum mechanical analysis.

Order No.: JA511-031

© 1995 MRS

Further Analysis of the Size Effect in Indentation Hardness Tests of Some Metals

M. Atkinson

(Jamberoo, Australia)

The variation of apparent hardness observed in previously reported Vickers indentation tests of metals is re-examined. Common descriptions of the effect are shown to be inaccurate: the variation of apparent hardness is monotonic but not simple. The effect is consistent with varying size of a previously postulated 'plastic hinge' at the perimeter of the indent. This complexity confers uncertainty on the estimation of characteristic macrohardness from small scale tests. Association of the indentation size effect with friction and with strain hardening is confirmed.

Order No.: JA511-032

© 1995 MRS

Interstitial Diffusion Along Twist Grain Boundaries in Cu

M. Nomura, J.B. Adams

(University of Illinois-Urbana)

Interstitial diffusion along twist grain boundaries was studied using the embedded atom method (EAM). Six (100) twist grain boundaries (8.79°-43.6°) in copper were investigated. Interstitial formation energies were found to be much lower (0.26-0.78 eV) than in the bulk, and migration energies were found to be comparable (0.01 eV-0.24 eV) to the bulk values (0.09 eV). The vacancy mechanism is favored for low angle boundaries and the interstitial mechanism is favored for high angle boundaries. The trends in formation energy vs. twist angle were partly explained in terms of the volume expansion of the grain boundary. The total diffusion rate due to both mechanisms was calculated and agreed reasonably with experimental data for Cu in polycrystalline Cu. The calculated diffusion rate for specific twist boundaries also agreed well with experimental measurements for Zn/Al.

Order No.: JA511-033

© 1995 MRS

Influence of Whisker Volume Fraction on the Creep Behavior of Alumina Composites Reinforced with Silicon Carbide

K. Xia*, T.G. Langdon*

(*University of Melbourne, *University of Southern California)

Four-point bending creep tests were conducted in air on two alumina matrix composites reinforced with 18 and 30 vol.% of silicon carbide whiskers, respectively. In both materials, the SiC whiskers tended to form agglomerates. In the temperature range from 1673 to 1823 K, the stress exponents, n , were ~3.9 and ~6.3 and the activation energies for creep, Q , were ~690-740 and ~930-1010 kJ mol⁻¹ for the composites containing 18 and 30 vol.% of SiC, respectively. It is shown that the higher value of n in the composite with 30 vol.% of SiC whiskers may be lowered to ~3 by incorporating a threshold stress. The creep strength of both composites was enhanced by comparison with a similar composite containing 9.3 vol.% of SiC whiskers, but there was only a very minor improvement in creep strength when the volume fraction of whiskers was increased from 18 to 30 vol.%.

Order No.: JA511-034

© 1995 MRS

Equilibrium Phase Diagrams in the System CuO-PbO-Ag

H.K. Liu*, S.X. Dou*, M. Ionescu*, Z.B. Shao*, K.R. Liu*, L.Q. Liu*

(*University of Wollongong, *Northeast University)

Silver has played a critical role for the fabrication of metal/high temperature superconductor composites. Phase equilibrium and microstructure in the ternary PbO-CuO-Ag system has been investigated using differential thermal analysis (DTA), thermogravimetry (TG), scanning electron microscope (SEM) and x-ray diffraction (XRD) techniques. Composition versus temperature diagrams have been established for these systems in air. In the ternary CuO-PbO-Ag system, there is a eutectic reaction $\text{CuO} + \text{PbO} + \text{Ag} = \text{L}$ at 750°C and a composition of 12.04% Mol Ag, 16.35% Mol CuO and 72.62% Mol PbO. Two immiscible regions near the two binary tie lines PbO-Ag and CuO-Ag were detected. No binary or ternary compound was detected in these systems. SEM and EDS results confirm the presence of two liquid phases and the eutectic point.

Order No.: JA511-035

© 1995 MRS

In-situ Reduction Kinetics of NiCl₂ in SiO₂ Gel Matrix

A. Basumallick*, K. Biswas*, G.C. Das*, S. Mukherjee*

(*Bengal Engineering College, *Jadavpur University)

Silica gels containing NiCl₂ and dextrose, have been reduced by heat treating the gels under N₂ atmosphere at 800°C, 850°C, 900°C and 950°C, respectively. The influence of volume ratio of ethyl alcohol to tetraethylorthosilicate and the amount of dextrose on the *in-situ* reduction kinetics of NiCl₂ in gel matrix have been investigated. The kinetic data on *in-situ* reduction have been analyzed by reduced time method which indicates that mixed mechanisms are operative. The predominant mechanism of reduction of NiCl₂ in SiO₂ gel matrix is of nucleation and growth type. The activation energies over different temperatures and fraction converted have been computed by integration method.

Order No.: JA511-036

© 1995 MRS

Elastic Properties of Sodium Borovanadate Glasses

S. Muthupari, S. Lakshmi Raghavan, K.J. Rao

(Indian Institute of Science)

The elastic properties of sodium borovanadate glasses have been studied over a wide range of composition using ultrasonic measurements. It is found that variation of different elastic moduli is very similar in any given series of composition. The bulk and the shear moduli show a monotonic variation with the covalent bond energy densities calculated from the proposed structural model for these glasses. The bulk moduli also varies as a negative power function of the mean atomic volume. The Debye temperature varies linearly with the glass transition temperature. The implications of the observed behavior have been discussed.

Order No.: JA511-037

© 1995 MRS

Controlling the Particle Size of Amorphous Iron NanoparticlesX. Cao, Yu. Kolytyn, G. Kataby, R. Prozorov, A. Gedanken
(Bar-Ilan University)

A method for controlling the particle size of amorphous iron which was prepared by the sonication of iron pentacarbonyl ($\text{Fe}(\text{CO})_5$) is reported in this paper. The sonolysis was performed on neat $\text{Fe}(\text{CO})_5$ and its solutions in decane whose concentrations were 4M, 1M and 0.25M. The iron nanoparticles were subjected to transmission electron micrograph (TEM), electron spin resonance (ESR), thermogravimetric analysis (TGA), differential scanning calorimetry (DSC) and Quantum Design SQUID magnetization measurement. The measured properties demonstrated a strong dependence on the concentration of the solution, e.g., particle size.

Order No.: JA511-038

© 1995 MRS

Morphology of α -Hexathieryl Thin-Film-Transistor FilmsA.J. Lovinger, D.D. Davis, R. Ruel, L. Torsi, A. Dodabalapur, H.E. Katz
(AT&T Bell Laboratories)

We have studied the morphology of thin films of α -hexathieryl (α -6T), a hexamer of thiophene that is a very promising material for thin-film-transistor applications. Using electron- and atomic-force microscopies, we found that on both rigid (Si/SiO_2 and glass) and flexible (polyimide) substrates, evaporated films show an apparently random, polycrystalline morphology. The crystals are lamellar, ca. 100–200 nm in lateral dimensions and 15–30 nm in thickness, and exhibit irregular boundaries. Nevertheless, electron-diffraction evidence from such films indicates that the constituent molecules are deposited preferentially end-

on and assume a normal or nearly normal orientation with respect to their substrates. Rapid high-temperature annealing causes growth of much larger (μm -sized) crystalline grains and a partial transformation to a high-temperature polymorph; however, this process leads to formation of gaps in the film, which may cause deterioration of electronic performance.

Order No.: JA511-039

© 1995 MRS

The Topaz to Mullite Transformation on Heating

R.A. Day*, E.R. Vance*, D.J. Cassidy*, J.S. Hartman*

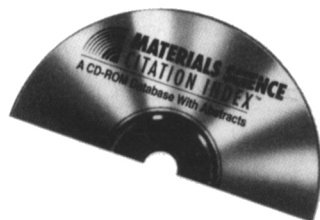
(*Australian Nuclear Science and Technology Organization, *Brock University)

The decomposition of topaz to mullite and other siliceous phases on heating above approximately 1100°C was found to depend on sample size and the presence of water vapor in the heating atmosphere. The principal experimental technique employed was scanning electron microscopy, but the data were supported by x-ray diffraction, thermal analysis, mass spectroscopy of volatile emissions, and solid-state nuclear magnetic resonance. In relatively large samples, the transformation to mullite evidently takes place by a vapor phase mechanism, within the bulk. The surface reaction which took place for samples heated in a wet atmosphere allowed the formation of high-silica glass, as well as mullite. The use of a hydrogenous heating atmosphere resulted in the sublimation and reformation of mullite whiskers, well outside the boundary of the original topaz.

Order No.: JA511-040

© 1995 MRS

Please use the convenient postcard located in the back of the *MRS Bulletin* to order *JMR* reprints. When ordering single article reprints please note they are not available until the issue is published.

NOW AVAILABLE FROM MRS**Materials Science Citation Index™****A CD-ROM Database with Abstracts**

A product of the Institute for Scientific Information®

Materials Science Citation Index (MSCI) provides researchers with extensive bibliographic information—including author, title, source publication, author-supplied abstract and cited references—from over 1300 books, journals and conference proceedings related to materials science. Total coverage exceeds 90,000 articles per year. Published bimonthly on compact disc, the **Materials Science Citation Index** covers all areas of materials science, including ceramics, semiconductors, superconductors, metals and metallurgy, thin films, plastics and polymer engineering, composites, biomaterials, adhesives, minerals, fabrics and fibers...plus electronics, surface science, applied physics, methods of extraction, processing and manufacturing, and more.

Unique features of the **MSCI** include: searchable author abstracts; cited reference searching, which enables you to take a known paper and find more recent papers that cite it; and Related Records™, which extends the power of citation indexing by linking and displaying the articles that have one or more references in common.

A 1995 subscription includes back-year data to 1991, for over 350,000 source items!

For more information contact:

Code: MSCI-B**\$799.00 MRS Members U.S.****\$ 994.00 Non-Members U.S.****\$819.00 MRS Members Foreign****\$1014.00 Non-Members Foreign****Free Sample Trial Available****MATERIALS RESEARCH SOCIETY**

Publications Department • 9800 McKnight Road • Pittsburgh, PA 15237-6006
Phone: 412-367-3012 • FAX: 412-367-4373